

Archaeometric analysis of patinas of the outdoor copper statue Sant'Oronzo (Lecce, Italy) preparatory to the restoration

Original

Archaeometric analysis of patinas of the outdoor copper statue Sant'Oronzo (Lecce, Italy) preparatory to the restoration / Buccolieri, G.; Castellano, A.; Serra, A.; Zavarise, G.; Palmiero, E.; Buccolieri, A.. - In: MICROCHEMICAL JOURNAL. - ISSN 0026-265X. - STAMPA. - 154:104538(2020). [10.1016/j.microc.2019.104538]

Availability:

This version is available at: 11583/2787076 since: 2020-01-30T14:41:25Z

Publisher:

Elsevier Inc.

Published

DOI:10.1016/j.microc.2019.104538

Terms of use:

This article is made available under terms and conditions as specified in the corresponding bibliographic description in the repository

Publisher copyright

(Article begins on next page)

1
2
3
4
5
6
7
8
9
10
11
12
13
14
15
16
17
18
19
20
21
22
23
24
25
26
27

Archaeometric analysis of *patinas* of the outdoor copper statue *Sant'Oronzo* (Lecce, Italy) preparatory to the restoration

Giovanni Buccolieri^a, Alfredo Castellano^a, Antonio Serra^a, Giorgio Zavarise^b,
Elisabetta Palmiero^c, Alessandro Buccolieri^{d,*}

^a Dipartimento di Matematica e Fisica, University of Salento, Lecce, Italy

^b Dipartimento di Ingegneria Strutturale, Edile e Geotecnica, Politecnico di Torino, Torino, Italy

^c Restauratrice dell'Azienda Colaci Emilio, Impianti e Restauri, Alessano, Lecce, Italy

^d Dipartimento di Scienze e Tecnologie Biologiche e Ambientali, University of Salento, Lecce, Italy

* Corresponding author. A. Buccolieri, Dipartimento di Scienze e Tecnologie Biologiche e Ambientali, University of Salento, Lecce, Italy. E-mail: alessandro.buccolieri@unisalento.it

Abstract

28 The *Sant'Oronzo* statue (Lecce, Southern Italy) consists of an internal wooden structure, completely
29 covered with copper sheets, lying on a concrete base about 1.5 meters high, which is placed on the
30 top of a Roman column about 29 meters high. Lecce may be classified as urban site since it is mainly
31 influenced by vehicular traffic and it is not affected by intense industrial emissions.

32
33 In the time schedule of the restoration, first of all, non-destructive analyses were planned. In
34 particular, a portable energy dispersive X-ray fluorescence (ED-XRF) was used in order to map the
35 composition of the *patinas* and to evaluate their degradation. Subsequently, a micro-sampling was
36 performed both of the statue and the column. The collected samples were analysed by using Raman
37 spectroscopy and X-Ray Diffraction in order to evaluate chemical composition.

38
39 This paper summarizes the archaeometric results and the diagnostic information obtained before of
40 the restoration, which are significant for the restorers' subsequent work.

41
42
43
44
45
46
47 **Keyword:** outdoor statue, copper, *patina*, ED-XRF, Raman, XRD

1. Introduction

48
49
50
51
52
53 The *patina* of outdoor copper manufacture has different chemical composition depending on the several
54 parameters such as alloy composition, environmental conditions (for instance, urban, rural, marine,
55 industrial), location of statue (in exposed areas or sheltered areas) and exposure time [1–4]. In
56
57
58
59

60 particular, in urban atmospheres, *patinas* directly exposed to rain are unstable and are leachable by
61 rainwaters.
62
63

64 The *patinas* spontaneously develop over time on copper and bronze surfaces due to chemical
65 reactions with the environment, creating corrosion compounds with various color (for example
66 green, red, bluish, brown and black) and different composition such as copper oxide, copper sulfide,
67 copper chloride, copper sulfate and copper carbonate [5–9]. In particular, the degradation compounds
68 most commonly found in copper manufactures are Cu_2O (cuprite), CuO (tenorite), Cu_2S (chalcocite),
69 CuS (covellite), CuCl (nantokite), $\text{CuCl}_2 \cdot 2\text{H}_2\text{O}$ (eriochalcite), $\text{Cu}_2\text{Cl}(\text{OH})_3$ (atacamite), $\text{Cu}_2\text{Cl}(\text{OH})_3$
70 (botallackite), $\text{Cu}_2\text{Cl}(\text{OH})_3$ (clinoatacamite), $\text{Cu}_3\text{SO}_4(\text{OH})_4$ (antlerite), $\text{Cu}_4\text{SO}_4(\text{OH})_6$ (brochantite),
71 Cu_2OSO_4 (dolerophanite), $\text{Cu}_4\text{SO}_4(\text{OH})_6 \cdot 2\text{H}_2\text{O}$ (langite), $\text{Cu}_4\text{SO}_4(\text{OH}) \cdot 6\text{H}_2\text{O}$ (posnjakite),
72 $\text{Cu}_4\text{SO}_4(\text{OH}) \cdot 2\text{H}_2\text{O}$ (wroewulfite), $\text{Cu}_2(\text{CO}_3)(\text{OH})_2$ (malachite), $\text{Cu}_3(\text{CO}_3)_2(\text{OH})_2$ (azurite) [10–12].
73
74 Jambor *et al.*, 1996 [13] reported for the first time the clinoatacamite, a new mineral polymorph of
75 $\text{Cu}_2\text{Cl}(\text{OH})_3$. Therefore, previous reports on paratacamite should probably be assigned to
76 clinoatacamite instead. The polymorphs $\text{Cu}_2\text{Cl}(\text{OH})_3$ (atacamite, paratacamite and clinoatacamite),
77 in combination with different hydroxy sulfates and cuprite, are dominant in the black sheltered areas,
78 while rain-washed green areas mainly consist of brochantite and cuprite [5,14,15].
79

80 The chemical composition of alloy and *patina* of copper or bronze can be determined using various
81 analytical methods such as energy dispersive X-ray fluorescence (ED-XRF), Raman spectroscopy,
82 scanning electron microscopy-energy dispersive X-ray (SEM-EDX), X-ray diffraction (XRD) and
83 atomic absorption spectroscopy (AAS). Nevertheless, methodologies often favoured in the field of
84 cultural heritage are non-destructive and portable techniques.
85

86 This work describes the experimental results of the diagnostic analysis performed on the
87 *Sant'Oronzo* statue (Lecce, Southern Italy) before starting the restoration in June 2018.
88

89 Lecce ($40^\circ 21' \text{ N}$; $18^\circ 10' \text{ E}$; 30 m above sea level) has about 95 thousand inhabitants and it is about
90 20 km away from both the Adriatic Sea and Ionian Sea. The town may be classified as urban site
91 since it is mainly influenced by vehicular traffic [16,17]. Fig. 1 shows some photos of the statue,
92 which highlight serious state of degradation of the copper sheet, of the Roman column and of the
93 concrete base.
94

95 2. Materials and methods

96 2.1. Description of statue

97 The *Sant'Oronzo* statue was built in Venice in 1739 and it is 4.90 meters high. It has an internal
98 wooden structure, completely covered with copper sheets, which were held together by copper nails.
99

119 The thickness of copper sheets is equal to about 1 mm. The original copper nails are about 2 to 5 cm
120 long (Fig. S1).
121
122

123 The statue is placed in *Sant'Oronzo* square, in the center of Lecce (Southern Italy), on a recent
124 concrete base (2.65 m × 2.65 m) about 1.5 meters high, which is positioned on a Roman column
125 about 29 meters high. The bottom of the statue is covered with a sheet of lead, which sit on the
126 concrete base.
127
128

129 The last restoration was performed in years 1982 to 1987. In the last restoration, several copper rivets
130 (with a steel nail, see Fig. S2) have been added to keep together the copper foils (Fig. S3).
131 Unfortunately, the use of these rivets induced galvanic corrosion phenomena, which are visible to the
132 naked eye. In fact, a close visual examination of statue allows to highlight two principal typologies
133 of *patinas*: light green *patina* (in areas exposed to leaching) and dark *patina* (in areas not exposed to
134 leaching), in addition to the numerous red drips, in correspondence of the rivets. Moreover, the
135 column shows both green and dark dripping on concrete basement and on Roman capital.
136
137
138
139

140 On January 30, 2019 the statue was removed and transferred for restoration to *Palazzo Carafa*, the
141 municipal building of Lecce, nearby the original site. Fig. S4 shows a picture of the statue in the
142 room where it will be restored.
143
144
145

146 2.2. Methods

147 2.2.1 ED-XRF

148
149
150 EDXRF portable equipment, which was assembled in our laboratory, is composed by an X-ray tube
151 (MOXTEK Inc., USA) with palladium anode air-cooled and by a detector Si-PIN (Amptek Inc.,
152 USA). The detector has a resolution of energy of about 180 eV at 5.9 keV. The output of the X-ray
153 tube is collimated and the analyzed area has a diameter of about 3 mm [18,19]. For each measuring
154 point, three EDXRF spectra were acquired, with acquisition time of 60 seconds and with a tube
155 voltage of 6 kV at 40 μA and of 20 kV at 3 μA.
156
157
158
159
160
161
162

163 Five standard samples, with known chemical compositions, were used to calibrate the apparatus and
164 to obtain reliable experimental data. For standards preparation, copper (II) sulphate pentahydrate
165 ($\text{CuSO}_4 \cdot 5\text{H}_2\text{O}$), copper (II) chloride dihydrate ($\text{CuCl}_2 \cdot 2\text{H}_2\text{O}$), copper (I) oxide (Cu_2O), copper (II)
166 sulfide (CuS) and iron powder have been used. All chemical compounds were purchased from
167 Sigma-Aldrich® with analytical grade.
168
169
170

171 Each standard was prepared by mixing the compounds in different weight percentages. The use of
172 different compounds with the same elements, but in different oxidation state, is irrelevant from the
173 point of view of the XRF analysis, but has allowed to obtain the calibration samples at different
174
175
176
177

178 concentrations. In particular, the chemicals compounds have been weighted by using an analytical
179 balance KERN model ABT 100-5M, subsequently mixed and homogenized in an agate mortar for
180 ten minutes and finally compressed at 200 bar for ten minutes. The homogeneity of elements in the
181 standard meets the requirements for the EDXRF quantitative analysis. Moreover, the samples
182 analysed are supposed to “*infinite thickness*” and therefore the quantitative results are expressed in
183 terms of weight percentage (% wt).

184 Copper, sulphur, chlorine and iron were determined, for each measurement point, in order to
185 individuate the chemical composition of the *patinas*. The description of each measurement point is
186 summarized in [Table 1](#). The values of detection limit, all reported in wt %, for copper, sulphur,
187 chlorine and iron are equal to 1.0, 0.5, 0.5 and 0.5 respectively. The software Microcal Origin
188 Professional® has been used to elaborate the experimental data obtained [20].

198 **2.2.2 Raman spectroscopy**

199 Raman analysis was performed on seven samples to identify *patina* composition. [Fig. 1](#) shows the
200 sampling point of each sample whose characteristics are described in [Table 2](#). The samples were
201 pounded to a fine powder in an agate mortar, homogenized and subsequently analyzed. Raman
202 analyses were achieved by using a spectrometer Renishaw model Invia (spectral resolution: 0.5 cm^{-1} ;
203 spectral range: $100 - 3700\text{ cm}^{-1}$) with an argon-ion laser ($\lambda = 514.5\text{ nm}$) and a LEICA
204 metallographic microscope. The laser beam was focused on the sample with 15 mW of excitation
205 power. The spectra were acquired for 20 accumulations by 100 s and repeated on five different
206 points. Then an average of Raman spectra was obtained. The spectra were obtained with baseline
207 correction and compared with standard spectra from the database www.ruff.info (atacamite
208 R050098, brochantite R060133, calcite R040170, cuprite R050384, graphite R050503, gypsum
209 R040029, murdochite R110122).

220 **2.2.3 XRD**

221 The XRD analyses were performed on the same samples examined with Raman spectroscopy. The
222 samples were analysed by using a diffractometer Rigaku model Mini Flex with Cu-K α radiation ($\lambda =$
223 0.154 nm). The measurements were carried out with 30 kV accelerating voltage, 15 mA current, scan
224 angle in 2θ from 10° to 80° , with step size of 0.01° and scan speed of $0.05^\circ\cdot\text{s}^{-1}$. Three scans for each
225 measurement were performed. XRD patterns were manually compared with standards XRD patterns
226 from the database www.ruff.info (atacamite R050098, brochantite R060133, calcite R040170,
227 cuprite R050384, graphite R050503, gypsum R040029, murdochite R110122).

3. Result and Discussion

3.1 ED-XRF analysis

Experimental results of ED-XRF analysis carried out on the *patinas* of the *Sant'Oronzo* statue are summarized in [Table 1](#).

Green *patina*, exposed to leaching (sample n. 01), shows copper (65 ± 2 % wt) as main element and sulphur (20 ± 2 % wt) as secondary element. Green *patina* on the mantle (sample n. 09) and the greenish dripping on the right arm (sample n. 06) have different composition.

Dark *patinas*, not exposed to leaching (samples n. 05, 07, 10, 11, 13 and 15), shows copper as main element and chlorine as secondary element. Moreover, the dark *patina* with red dripping on the bottom right mantle (sample n. 12) shows higher sulphur concentration (11.5 ± 1.0 % wt) and iron (1.5 ± 0.5 % wt) as in trace element. Red *patinas*, exposed to leaching (samples n. 02, 03 and 04), show copper and iron as main element and sulphur as secondary element.

It is important to note that iron is widely present on the surface of statue as minor element or in trace. This is due to the corrosion of the rivets nails added during the last restoration accomplished from 1982 to 1987. In fact, the recent rivet (sample n. 19) shows copper (39 ± 2 % wt) as main element and iron (10.0 ± 1.0 % wt) as secondary element, whereas the rivet (sample n. 20) shows iron (27 ± 2 % wt) as main element and copper (12.0 ± 1.0 % wt) as secondary element.

The original nails show copper (45-56 % wt) as main element. Moreover, the nail n. 16 and n. 18 show chlorine (21 ± 2 % wt) as secondary element, while the nail n. 17 shows sulphur (12.0 ± 1.0 % wt) and chlorine (5.0 ± 0.5 % wt) as secondary elements.

Cleaning tests were also carried out on some measuring points both on areas of the statue (sample n. 01 and n. 15) and on nails (sample n. 16, n. 17 and n. 18) and on rivets (sample n. 19). In any case, the increase of copper concentration was highlighted with a simultaneous decrease in sulphur and chlorine concentration.

3.2 Raman and XRD analysis

Raman spectroscopy offers chemical identification of compounds in order to discriminate the corrosion products of copper or bronze manufacture [6,21–25]. In particular, the Raman signals of copper hydroxychlorides and copper hydroxysulphates can be observed in two main regions: the first at lower wavenumbers, between 100 cm^{-1} and 1100 cm^{-1} , includes Cu–O deformation, Cu–Cl deformation and SO_4^{2-} deformation. The second, at high wavenumbers, between 3000 cm^{-1} and 3700

296 cm⁻¹, includes the Cu–O–H stretching vibrations. In particular, the number of bands in this region
297 usually reflects the number of different O–H groups present in the structure, except in the case of
298 strong overlap of the bands. For instance, brochantite (Cu₄SO₄(OH)₆) has six hydroxyl groups
300 bonded to adjacent sulphate group, and therefore Raman spectroscopy shows six peaks. There is
301 another region, between 1100 cm⁻¹ and 3700 cm⁻¹, which includes the signals that characterize the
302 amorphous carbon [26–28], often determined on outdoor copper monuments, as well as C–H
303 vibrations of organic compounds and the water features present in several hydrated mineral phases.
304
305
306
307

308 In Table 3 it was tried to assign the type of deformation for each Raman signal obtained in analysed
309 *patinas* of the statue.
310

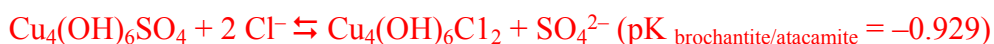
311 Fig. 2a shows the comparison between the Raman spectrum of the green *patina* and of the standard
312 brochantite. Raman spectrum of green *patina* has the following signals: 120, 140, 200, 242, 318, 390,
313 420, 450, 485, 506, 595, 609, 622, 910, 975, 1075, 1095, 1125, 1350, 1580, 3265, 3375, 3402, 3489,
314 3565, 3588 cm⁻¹. According to the data reported by scientific literature [29–35] all signals of green
315 *patina* are attributable to brochantite, except two peaks broader with Raman shift values of about
316 1350 cm⁻¹ and 1580 cm⁻¹, which are attributable to amorphous carbon and are called D (disorder
317 band) and G (graphitic band) band, respectively. Moreover, the spectrum of green *patina* shows a
318 broad band in the range 2800–3000 cm⁻¹, which is the region of C–H vibrations of saturated organic
319 molecules, mainly hydrocarbons and carboxylic acids.
320
321
322
323
324

325 Fig. 3a shows the comparison between the Raman spectrum of the dark *patina* and of the standard
326 atacamite (Cu₂Cl(OH)₃). Raman spectrum of dark *patina* has the following signals: 220, 415, 510,
327 635, 810, 905, 980, 1340, 1600, 2915, 3200, 3355, 3435 cm⁻¹. In according to the data reported by
328 scientific literature, all signals of dark *patina* are attributable to atacamite, in addition to the presence
329 of amorphous carbon. Moreover, the spectrum shows two broad bands in the range 2800–3000 cm⁻¹,
330 which are the region of C–H vibrations of saturated organic molecules, mainly hydrocarbons and
331 carboxylic acids.
332
333
334
335
336

337 Fig. 4a shows the comparison between the typical Raman spectrum of the sample C04 (green
338 dripping on Roman capital, West side) and of the standard calcite (CaCO₃). Raman spectrum of
339 sample C04 has the following signals: 155, 285, 715, 1085, 1435, 1750, 2625, 2670, 3220 and 3470
340 cm⁻¹. This comparison demonstrated that the sample is mainly composed of calcite and the signals
341 relating C–H vibrations of saturated organic molecules.
342
343
344

345 XRD analysis prove that both the green *patina* (Fig. 2b) and the dark *patina* (Fig. 3b) contain cuprite
346 (2θ equal to 29.6, 36.5, 42.3, 61.4, 73.5 and 77.4). This oxide represents the protective layer that
347 normally covers outdoor copper and bronze monuments. In addition, green *patina* is characterized by
348 the presence of brochantite, whereas dark *patina* is characterized mainly by the presence of atacamite
349 more brochantite.
350
351
352
353
354

355
356 Several studies have shown that brochantite is converted into atacamite in solutions containing high
357 levels of chloride ions through a mechanism of dissolution and precipitation. This chemical-physical
358 process is reasonable considering the different solubility of the two compounds and their stability
359 ratio:
360



364
365
366 XRD pattern of the sample C01 (dark dripping on concrete pulvino) shows the presence mainly of
367 calcite and gypsum, typical compounds used in cementitious material in the form of powders, and of
368 murdochite (Cu_6PbO_8). Fig. S5 shows the XRD spectrum of sample C01. The existence of
369 murdochite on pulvino can be justified considering the corrosion of the lead plate placed at the
370 pedestal of the statue on which the wooden structure rests.
371

372
373
374 XRD pattern of the sample C02 (green dripping on concrete pulvino) shows the presence mainly of
375 calcite. The weak signal at 2θ equal to 16.2° is due to atacamite, confirming that its drip from the
376 copper statue is the cause of the green coloured areas. The sample C03 (dark dripping on Roman
377 capital) is also characterized by the presence of calcite as main phase. The dark colour is due both to
378 the presence of carbon particles and to a dripping of murdochite that comes from the statue's
379 pedestal. The sample C04 (green dripping on Roman capital) is mainly characterized by calcite (Fig.
380 4b). The light green colouring on the capital could be due to brochantite of coming from the metallic
381 statue.
382

383
384
385 The sample C05 (dark area not exposed to washouts on Roman capital) shows the presence of
386 gypsum as the main phase and calcite. The graphite signal is also present and this may be due to
387 carbon particles deposited in not washed region, which determine the dark colour.
388

389
390
391 The results obtained by using XRD confirm the results obtained by Raman spectroscopy.
392

393 394 395 396 **4. Conclusion**

397
398
399
400 Green *patinas* were constituted mainly by cuprite and brochantite, while dark *patinas* were
401 constituted mainly by cuprite, brochantite and atacamite. The presence of atacamite in areas not
402 directly exposed to rain may be due probably to deposits of marine spray accumulated in these
403 sheltered regions of the statue.
404

405
406 Furthermore, all the *patinas* contain amorphous carbon which demonstrates the presence of carbon
407 deposits. In particular, the highest concentration of amorphous carbon was detected in the sheltered
408 dark *patinas*.
409

414
415 The improper use of the rivets used in the last restoration from 1982 to 1987 has irreversibly
416 damaged the analysed monument, thus modifying its aesthetics (with evident red areas around each
417 rivet and red dripping starting from the rivet).
418

419
420 The simultaneous use of the analytical techniques has allowed to define the compounds of
421 degradation of *patinas* and the information obtained was of fundamental importance for the
422 subsequent work of the restorers.
423
424

425 426 **Acknowledgments**

427
428
429 The authors thank Massimo Luggeri (Dipartimento di Scienze e Tecnologie Biologiche e Ambientali,
430 Università del Salento), who has contributed to improving the quality of the figures. We are grateful
431 to Company Colaci Emilio Impianti e Restauri (Alessano, Lecce, Italy) and the restorer Elisabetta
432 Palmiero for promoting this study and for his continuous collaboration. We are also very grateful to
433 Arch. Maria Piccarreta (*Soprintendenza archeologia belle arti e paesaggio per le province di*
434 *Brindisi, Lecce e Taranto*) for her always collaborative attitude.
435
436
437
438
439

440 441 **References**

- 442
443 [1] G.M. Ingo, T. De Caro, C. Riccucci, E. Angelini, S. Grassini, S. Balbi, P. Bernardini, D. Salvi, L.
444 Bousselmi, A. Çilingiroğlu, M. Gener, V.K. Gouda, O.A.L. Jarrah, S. Khosroff, Z. Mahdjoub, Z.A.L.
445 Saad, W. El-Saddik, P. Vassiliou, Large scale investigation of chemical composition, structure and
446 corrosion mechanism of bronze archeological artefacts from Mediterranean basin, *Appl. Phys. A*
447 *Mater. Sci. Process.* 83 (2006) 513–520. doi:10.1007/s00339-006-3550-z.
448 [2] D.E. Couture-Rigert, P.J. Sirois, E.A. Moffatt, An investigation into the cause of corrosion on indoor
449 bronze sculpture, *Stud. Conserv.* 57 (2012) 142–163. doi:10.1179/2047058412Y.0000000004.
450 [3] X. Zhang, I. Odnevall Wallinder, C. Leygraf, Mechanistic studies of corrosion product flaking on
451 copper and copper-based alloys in marine environments, *Corros. Sci.* 85 (2014) 15–25.
452 doi:10.1016/j.corsci.2014.03.028.
453 [4] G. Masi, J. Esvan, C. Josse, C. Chiavari, E. Bernardi, C. Martini, M.C. Bignozzi, N. Gartner, T. Kosec,
454 L. Robbiola, Characterization of typical patinas simulating bronze corrosion in outdoor conditions,
455 *Mater. Chem. Phys.* 200 (2017) 308–321. doi:10.1016/j.matchemphys.2017.07.091.
456 [5] R.A. Livingston, Influence of the Environment on the Patina of the Statue of Liberty, *Environ. Sci.*
457 *Technol.* 25 (1991) 1400–1408. doi:10.1021/es00020a006.
458 [6] W. Martens, R.L. Frost, J.T. Kloprogge, P.A. Williams, Raman spectroscopic study of the basic copper
459 sulphates - Implications for copper corrosion and “bronze disease,” *J. Raman Spectrosc.* 34 (2003)
460 145–151. doi:10.1002/jrs.969.
461 [7] R.L. Frost, P.A. Williams, J.T. Kloprogge, W. Martens, Raman spectroscopy of the copper chloride
462 minerals nantokite, eriochalcite and claringbullite – implications for copper corrosion, *Neues Jahrb.*
463 *Für Mineral. - Monatshefte.* 2003 (2003) 433–445. doi:10.1127/0028-3649/2003/2003-0433.
464 [8] V. Hayez, V. Costa, J. Guillaume, H. Terryn, A. Hubin, Micro Raman spectroscopy used for the study
465 of corrosion products on copper alloys: Study of the chemical composition of artificial patinas used for
466 restoration purposes, *Analyst.* 130 (2005) 550–556. doi:10.1039/b419080g.
467 [9] X.D. Liu, D.D. Meng, X.G. Zheng, M. Hagihala, Q.X. Guo, Mid-IR and Raman Spectral Properties of
468 Clinoatacamite-Structure Basic Copper Chlorides, *Adv. Mater. Res.* 146–147 (2010) 1202–1205.
469 doi:10.4028/www.scientific.net/AMR.146-147.1202.
470 [10] A.R. Mendoza, F. Corvo, A. Gómez, J. Gómez, Influence of the corrosion products of copper on its
471 atmospheric corrosion kinetics in tropical climate, *Corros. Sci.* 46 (2004) 1189–1200.
472

- 473
474
475
476
477
478
479
480
481
482
483
484
485
486
487
488
489
490
491
492
493
494
495
496
497
498
499
500
501
502
503
504
505
506
507
508
509
510
511
512
513
514
515
516
517
518
519
520
521
522
523
524
525
526
527
528
529
530
531
- doi:10.1016/j.corsci.2003.09.014.
- [11] A.M. Pollard, R.G. Thomas, P.A. Williams, Connellite : stability relationships with other secondary copper minerals, 54 (1990) 425–430.
- [12] G. Di Carlo, C. Giuliani, C. Riccucci, M. Pascucci, E. Messina, G. Fierro, M. Lavorgna, G.M. Ingo, Artificial patina formation onto copper-based alloys: Chloride and sulphate induced corrosion processes, *Appl. Surf. Sci.* 421 (2017) 120–127. doi:10.1016/j.apsusc.2017.01.080.
- [13] J.T. Jambor, John L.; Dutrizac, John E.; Roberts, Andrew C.; Grice, Joel D.; Szymanski, Clinoatacamite, a new polymorph of $\text{Cu}_2(\text{OH})_3\text{Cl}$, and its relationship to paratacamite and “anarakite,” *Can. Mineral.* 34 (1996) 61–72.
- [14] R.W. Revie, Uhlig ' S Corrosion Handbook the Electrochemical Society Series, 2011. doi:10.1002/9780470872864.ch39.
- [15] L.S. Selwyn, N.E. Binnie, J. Poitras, M.E. Laver, D.A. Downham, Outdoor Bronze Statues: Analysis of Metal and Surface Samples, *Stud. Conserv.* 41 (1996) 205. doi:10.2307/1506541.
- [16] M. Rita Perrone, A. Turnone, A. Buccolieri, G. Buccolieri, Particulate matter characterization at a coastal site in south-eastern Italy, *J. Environ. Monit.* 8 (2006) 183–190. doi:10.1039/B513306H.
- [17] A. Buccolieri, G. Buccolieri, N. Cardellicchio, A. Dell'Atti, E.T. Florio, PM-10 and heavy metals in particulate matter of the province of Lecce (Apulia, Southern Italy), *Ann. Chim.* 95 (2005). doi:10.1002/adic.200590004.
- [18] A. Buccolieri, A. Castellano, E. Degl'Innocenti, R. Cesareo, R. Casciaro, G. Buccolieri, EDXRF analysis of gold jewelry from the Archaeological Museum of Taranto, Italy, *X-Ray Spectrom.* 46 (2017). doi:10.1002/xrs.2761.
- [19] A. Buccolieri, E. Degl'Innocenti, R. Cesareo, A. Castellano, G. Buccolieri, Non-invasive in-situ analysis of a wreath of gold leaves from the National Archaeological Museum of Taranto, Italy, *Meas. J. Int. Meas. Confed.* 126 (2018) 164–167. doi:10.1016/j.measurement.2018.05.063.
- [20] G. Buccolieri, A. Buccolieri, P. Donati, M. Marabelli, A. Castellano, Nuclear Instruments and Methods in Physics Research B Portable EDXRF investigation of the patinas on the Riace Bronzes, *Nucl. INSTRUMENTS METHODS Phys.* 343 (2015) 101–109. doi:10.1016/j.nimb.2014.11.064.
- [21] R.L. Frost, W. Martens, J. Theo Kloprogge, P.A. Williams, Raman spectroscopy of the basic copper chloride minerals atacamite and paratacamite: Implications for the study of copper, brass and bronze objects of archaeological significance, *J. Raman Spectrosc.* 33 (2002) 801–806. doi:10.1002/jrs.921.
- [22] R.L. Frost, W.N. Martens, L. Rintoul, E. Mahmutagic, J.T. Kloprogge, Raman spectroscopic study of azurite and malachite at 298 and 77 K, *J. Raman Spectrosc.* 33 (2002) 252–259. doi:10.1002/jrs.848.
- [23] R.L. Frost, P.A. Williams, W. Martens, P. Leverett, J.T. Kloprogge, Raman spectroscopy of basic copper(II) and some complex copper(II) sulfate minerals: Implications for hydrogen bonding, *Am. Mineral.* 89 (2004) 1130–1137. doi:10.2138/am-2004-0726.
- [24] G. Bertolotti, D. Bersani, P.P. Lottici, M. Alesiani, T. Malcherek, J. Schlüter, Micro-Raman study of copper hydroxychlorides and other corrosion products of bronze samples mimicking archaeological coins, *Anal. Bioanal. Chem.* 402 (2012) 1451–1457. doi:10.1007/s00216-011-5268-9.
- [25] R.L. Frost, R. Scholz, A. López, Y. Xi, C. Lana, Vibrational spectroscopy of the sulphate mineral sturmanite from Kuruman manganese deposits, South Africa, *Spectrochim. Acta - Part A Mol. Biomol. Spectrosc.* 133 (2014) 24–30. doi:10.1016/j.saa.2014.04.115.
- [26] T. Catelani, G. Pratesi, M. Zoppi, Raman characterization of ambient airborne soot and associated mineral phases, *Aerosol Sci. Technol.* 48 (2014) 13–21. doi:10.1080/02786826.2013.847270.
- [27] C. Brolly, J. Parnell, S. Bowden, Raman spectroscopy: Caution when interpreting organic carbon from oxidising environments, *Planet. Space Sci.* 121 (2016) 53–59. doi:10.1016/j.pss.2015.12.008.
- [28] A. Coccato, J. Jehlicka, L. Moens, P. Vandenabeele, Raman spectroscopy for the investigation of carbon-based black pigments, *J. Raman Spectrosc.* 46 (2015) 1003–1015. doi:10.1002/jrs.4715.
- [29] M. Schmidt, H.D. Lutz, Hydrogen bonding in basic copper salts: a spectroscopic study of malachite, $\text{Cu}_2(\text{OH})_2\text{CO}_3$, and brochantite, $\text{Cu}_4(\text{OH})_6\text{SO}_4$, *Phys. Chem. Miner.* 20 (1993) 27–32. doi:10.1007/BF00202247.
- [30] M. Bouchard, D.C. Smith, Catalogue of 45 reference Raman spectra of minerals concerning research in art history or archaeology, especially on corroded metals and coloured glass, *Spectrochim. Acta - Part A Mol. Biomol. Spectrosc.* 59 (2003) 2247–2266. doi:10.1016/S1386-1425(03)00069-6.
- [31] R.L. Frost, Raman spectroscopy of selected copper minerals of significance in corrosion, *Spectrochim. Acta - Part A Mol. Biomol. Spectrosc.* 59 (2003) 1195–1204. doi:10.1016/S1386-1425(02)00315-3.
- [32] P. Makreski, G. Jovanovski, S. Dimitrovska, Minerals from Macedonia: XIV. Identification of some sulfate minerals by vibrational (infrared and Raman) spectroscopy, *Vib. Spectrosc.* 39 (2005) 229–239.

532
533
534
535
536
537
538
539
540
541
542
543
544
545
546
547
548
549
550
551
552
553
554
555
556
557
558
559
560
561
562
563
564
565
566
567
568
569
570
571
572
573
574
575
576
577
578
579
580
581
582
583
584
585
586
587
588
589
590

doi:10.1016/j.vibspec.2005.04.008.

- [33] M.D. Lane, Mid-infrared emission spectroscopy of sulfate and sulfate-bearing minerals, *Am. Mineral.* 92 (2007) 1–18. doi:10.2138/am.2007.2170.
- [34] K. Ben Mabrouk, T.H. Kauffmann, H. Aroui, M.D. Fontana, Raman study of cation effect on sulfate vibration modes in solid state and in aqueous solutions, *J. Raman Spectrosc.* 44 (2013) 1603–1608. doi:10.1002/jrs.4374.
- [35] A. Coccato, D. Bersani, A. Coudray, J. Sanyova, L. Moens, P. Vandenabeele, Raman spectroscopy of green minerals and reaction products with an application in Cultural Heritage research, *J. Raman Spectrosc.* 47 (2016) 1429–1443. doi:10.1002/jrs.4956.

AUTHOR INFORMATION

ORCID ID:

Buccolieri Giovanni: <http://orcid.org/0000-0001-8672-9238>

Alfredo Castellano: <http://orcid.org/0000-0002-3107-5836>

Antonio Serra: <http://orcid.org/0000-0003-3380-7751>

Giorgio Zavarise: <http://orcid.org/0000-0002-6340-0015>

Buccolieri Alessandro: <http://orcid.org/0000-0002-8657-9468>

591
592 **Caption of the Figures**
593
594

595 **Fig. 1.** Images of the *Sant'Oronzo* statue (a) and degraded areas of copper *patinas* (b, c and d), of the
596 Roman column (e, f and g) and the concrete base (h). The figure also shows the seven sampling
597 points, which provided the samples analysed both with Raman and XRD.
598

599 **Fig. 2.** Typical Raman spectrum (a) and XRD pattern (b) of the green *patina* compared with
600 brochantite standard.
601

602 **Fig. 3.** Typical Raman spectrum (a) and XRD pattern (b) of the dark *patina* compared with atacamite
603 standard.
604

605 **Fig. 4.** Typical Raman spectrum (a) and XRD pattern (b) of the sample C04 compared with calcite
606 standard.
607

608 **Fig. S1.** Image from above (a) and front (b) of the original nails of the *Sant'Oronzo* statue.
609

610 **Fig. S2.** Rivet fixing technique.
611

612 **Fig. S3.** Image of evidence of rivets on the statue.
613

614 **Fig. S4.** Image of the *Sant'Oronzo* statue in the room where it will be restored.
615

616 **Fig. S5.** XRD pattern of the sample C01.
617
618
619
620

621 **Caption of the Tables**
622
623
624

625 **Table 1.** ED-XRF analysis results of different *patinas* on the *Sant'Oronzo* statue.
626

627 **Table 2.** Description of the seven samples analysed by Raman spectroscopy and XRD and main
628 compounds detected
629

630 **Table 3.** Raman peaks obtained from *patinas* on the *Sant'Oronzo* statue and their possible
631 assignment.
632
633
634
635
636
637
638
639
640
641
642
643
644
645
646
647
648
649

650
651
652
653
654
655
656
657
658
659
660
661
662
663
664
665
666
667
668
669
670
671
672
673
674
675
676
677
678
679
680
681
682
683
684
685
686
687
688
689
690
691
692
693
694
695
696
697
698
699
700
701
702
703
704
705
706
707
708

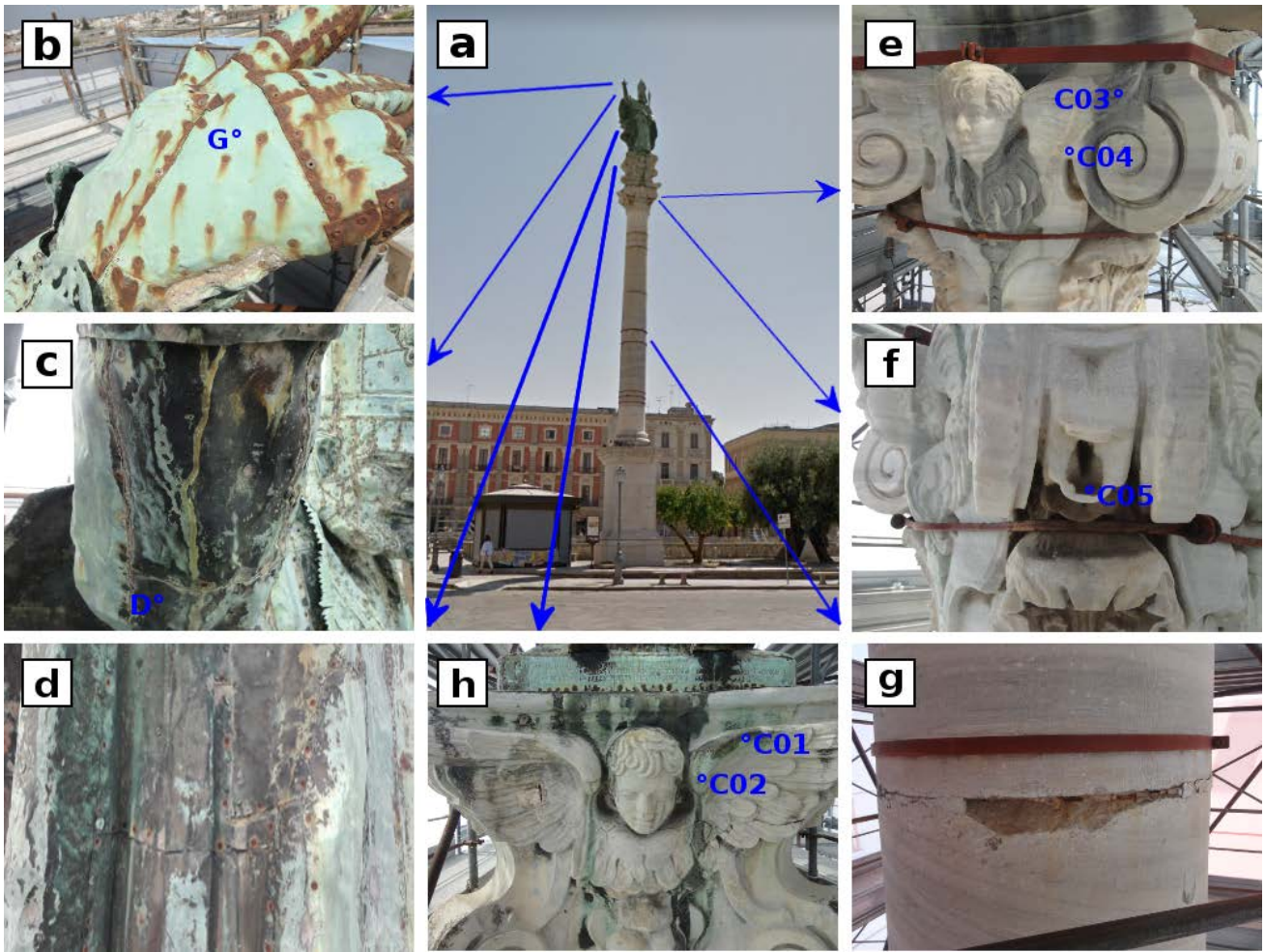
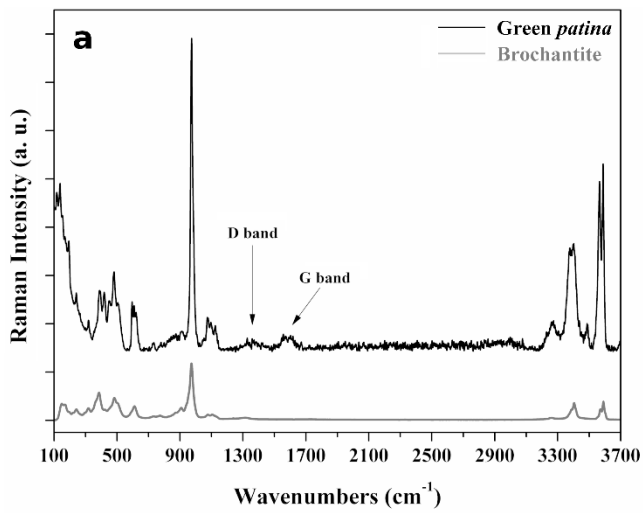
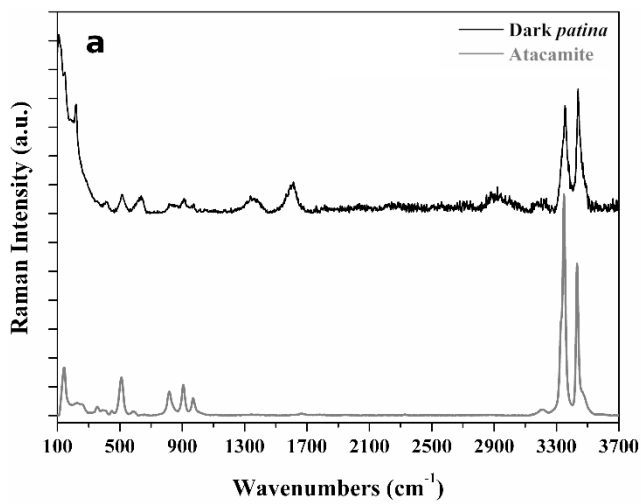


Fig. 1



726
727
728
729

Fig. 2



745
746
747
748
749

Fig. 3

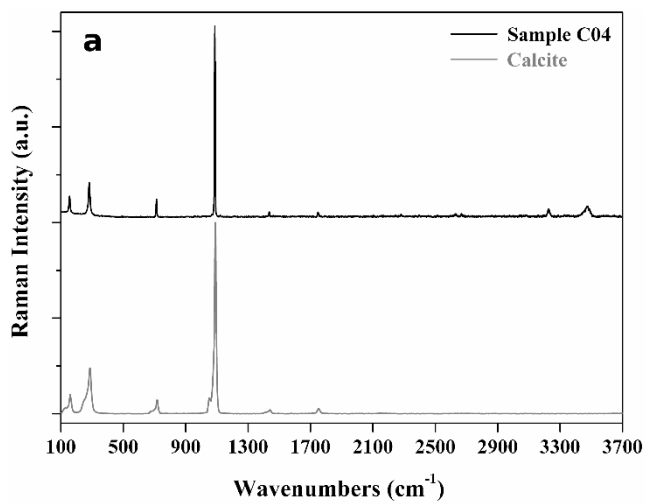


Fig. 4

768
769
770
771
772
773
774
775
776
777
778
779
780
781
782
783
784
785
786
787
788
789
790
791
792
793
794
795
796
797
798
799
800
801
802
803
804
805
806
807
808
809
810
811
812
813
814
815
816
817
818
819
820
821
822
823
824
825
826

Table 1

Sample	Description of sample	Cu	S	Cl	Fe
		(% wt)			
01	Right hand, green <i>patina</i> exposed to leaching	65±2	20±2	<0.5	<0.5
01c	Sample 01 <i>after cleaning</i>	89±2	2.5±0.5	<0.5	1.0±0.5
02	Right hand, red <i>patina</i> exposed to leaching	48.0±1.5	4.4±0.5	<0.5	23±2
03	Right hand, red dripping exposed to leaching	58±2	11.0±1.0	<0.5	4.5±0.5
04	Right hand, red sheet exposed to leaching	87±2	<0.5	<0.5	2.5±0.5
05	Right arm, dark <i>patina</i> sheltered area	50±2	<0.5	23±2	<0.5
06	Right arm, greenish dripping, sheltered area	49±2	17.0±1.5	3.5±0.5	4.0±0.5
07	Dark <i>patina</i> under the mantle, sheltered area	47±2	<0.5	20±2	<0.5
08	Hole on the arm	69±2	7.0±1.0	<0.5	10.0±1.0
09	Mantle, right side, green <i>patina</i> , flat surface	20±2	8.0±1.0	7.0±0.5	<0.5
10	Bottom right mantle, dark <i>patina</i>	45±2	<0.5	19.3±1.5	1.5±0.5
11	Right side, dark <i>patina</i> , sheltered area	48±2	<0.5	16.3±1.5	<0.5
12	Bottom right mantle, dark <i>patina</i> with red dripping	38±2	11.5±1.0	<0.5	1.5±0.5
13	Bottom right base, dark <i>patina</i>	41±2	5.0±0.5	14.0±1.5	<0.5
14	Right side, iron rod	<1.0	<0.5	<0.5	55±2
15	Brown <i>patina</i> , sheltered area	53±2	<0.5	11.0±1.0	<0.5
15c	Sample 15 <i>after cleaning</i>	92±2	<0.5	<0.5	<0.5
16	Right hand, original nail, exposed to leaching	56±2	<0.5	21±2	1.0±0.5
16c	Sample 16 <i>after cleaning</i>	90±2	<0.5	1.5±0.5	1.0±0.5
17	Original nail with green head	52±2	12.0±1.0	5.0±0.5	<0.5
17c	Sample 17 <i>after cleaning</i>	91±2	<0.5	<0.5	<0.5
18	Original nail with dark head	45±2	<0.5	21±2	<0.5
18c	Sample 18 <i>after cleaning</i>	91±2	<0.5	<0.5	<0.5
19	Right hand, recent red rivet, exposed to leaching	39±2	<0.5	1.0±0.5	10.0±1.0
19c	Sample 19 <i>after cleaning</i>	89±2	<0.5	<0.5	8.0±1.0
20	Right hand, red rivet, exposed to leaching	12.0±1.0	<0.5	<0.5	27±2

827
828
829
830
831
832
833
834
835
836
837
838
839
840
841
842
843
844
845
846
847
848
849
850
851
852
853
854
855
856
857
858
859
860
861
862
863
864
865
866
867
868
869
870
871
872
873
874
875
876
877
878
879
880
881
882
883
884
885

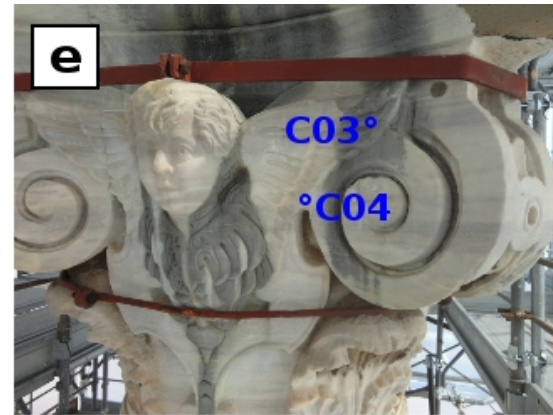
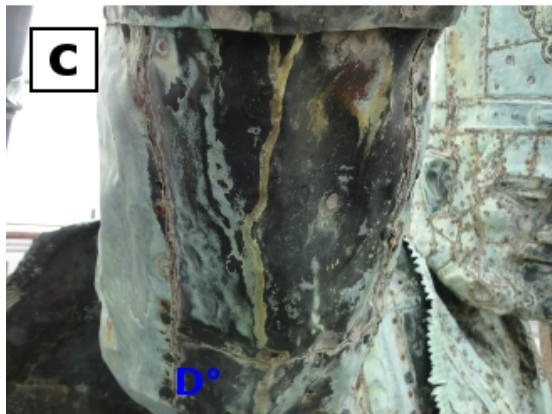
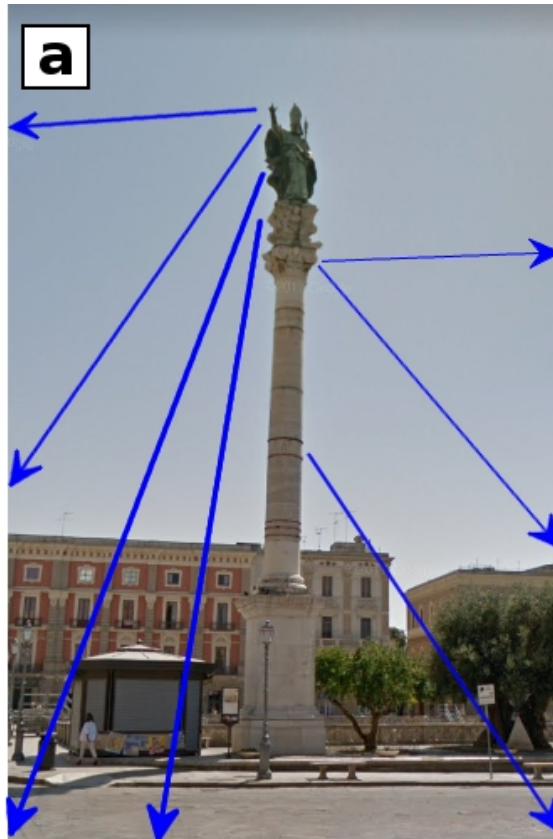
Table 2

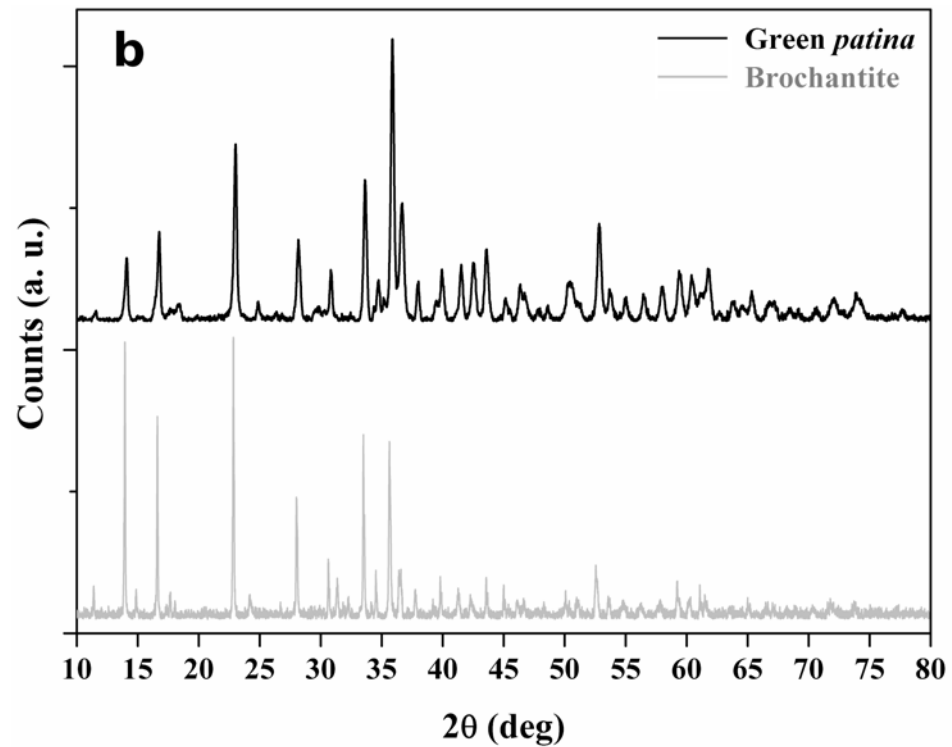
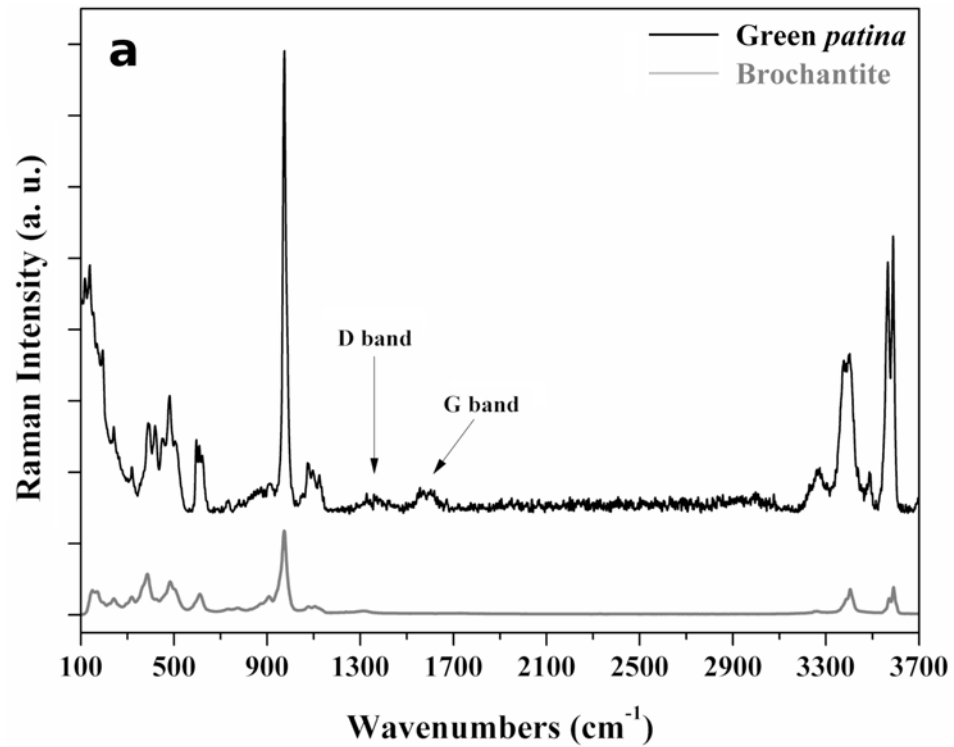
Sample	Description of sample	Main compounds determined	
		by Raman	by XRD
G	Right hand, green sheet, exposed to leaching	Brochantite	Brochantite, Cuprite
D	Right arm, dark sheet, sheltered area	Atacamite	Atacamite, Cuprite
C01	Dark dripping on concrete pulvino, South side	Calcite	Calcite, Gypsum, Murdochite
C02	Green dripping on concrete pulvino, South side	Calcite	Calcite, Atacamite
C03	Dark dripping on Roman capital, West side	Calcite	Calcite, Murdochite
C04	Green dripping on Roman capital, West side	Calcite	Calcite
C05	Dark area on Roman capital (volute), North-West side	Gypsum	Gypsum

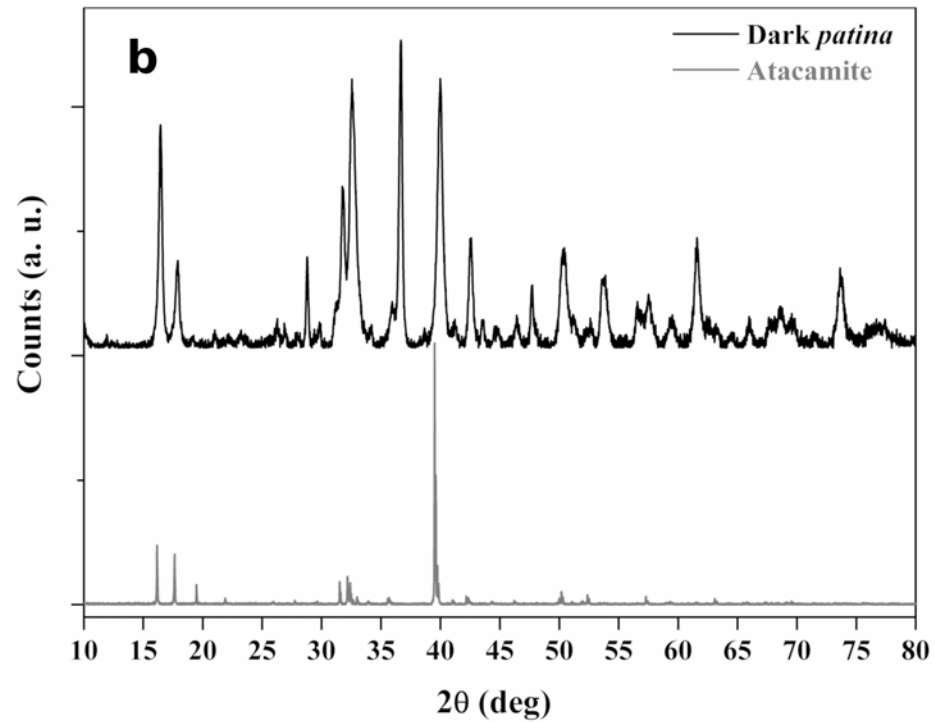
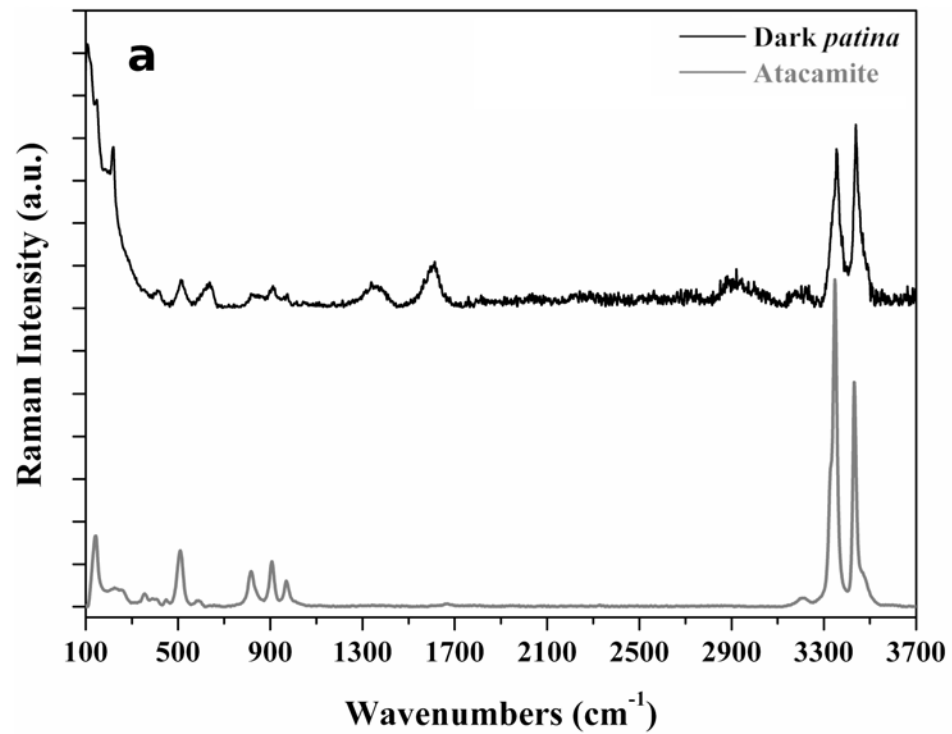
Table 3

886
887
888
889
890
891
892
893
894
895
896
897
898
899
900
901
902
903
904
905
906
907
908
909
910
911
912
913
914
915
916
917
918
919
920
921
922
923
924
925
926
927
928
929
930
931
932
933
934
935
936
937
938
939
940
941
942
943
944

Wavenumber (cm ⁻¹)	Suggested assignment
120 140	Cu–O bending
155	(Ca ²⁺ , CO ₃ ²⁻) lattice modes
200	Cu–Cl bending
225	Cu–O bending
242	Cu–Cl bending
285	(Ca ²⁺ , CO ₃ ²⁻) lattice modes
318 390 420	Cu–Cl stretching
450	SO ₄ ²⁻ symmetric bending
485 506	Cu–O symmetric stretching
520	Cu–OH symmetric stretching
595 609 622	SO ₄ ²⁻ anti-symmetric bending
625	Cu–O symmetric stretching
715	CO ₃ ²⁻ symmetric stretching
808 825 910 975	OH deformation
975	SO ₄ ²⁻ symmetric stretching
1075 1095 1125	SO ₄ ²⁻ anti-symmetric stretching
1085	CO ₃ ²⁻ symmetric stretching
1350	disorder carbon (<i>band D</i>)
1580	graphitic carbon (<i>band G</i>)
1435	CO ₃ ²⁻ asymmetric stretching
1750	CO ₃ ²⁻ symmetric stretching
3260 3375 3405 3490 3565 3585	Cu–OH hydroxyl stretching

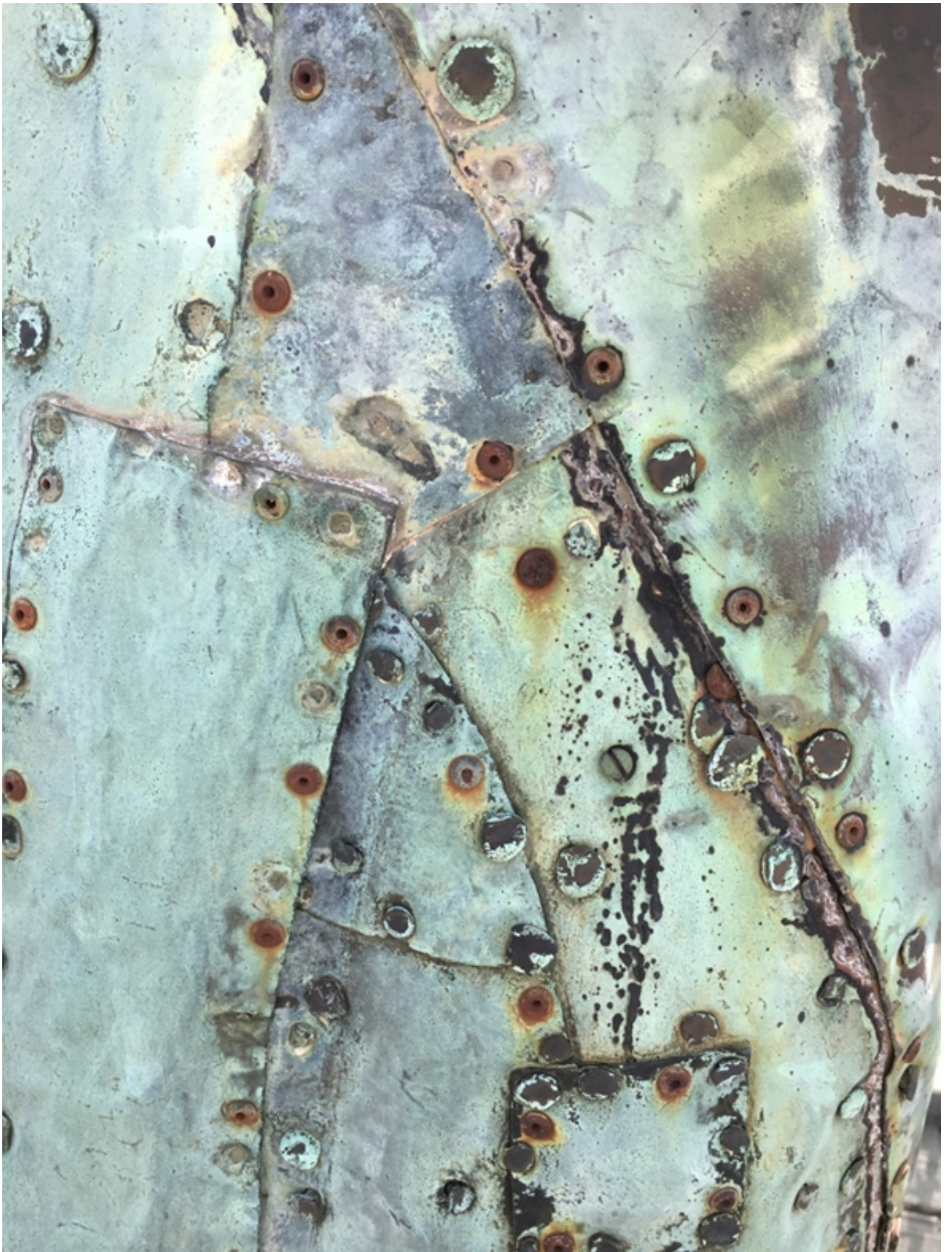




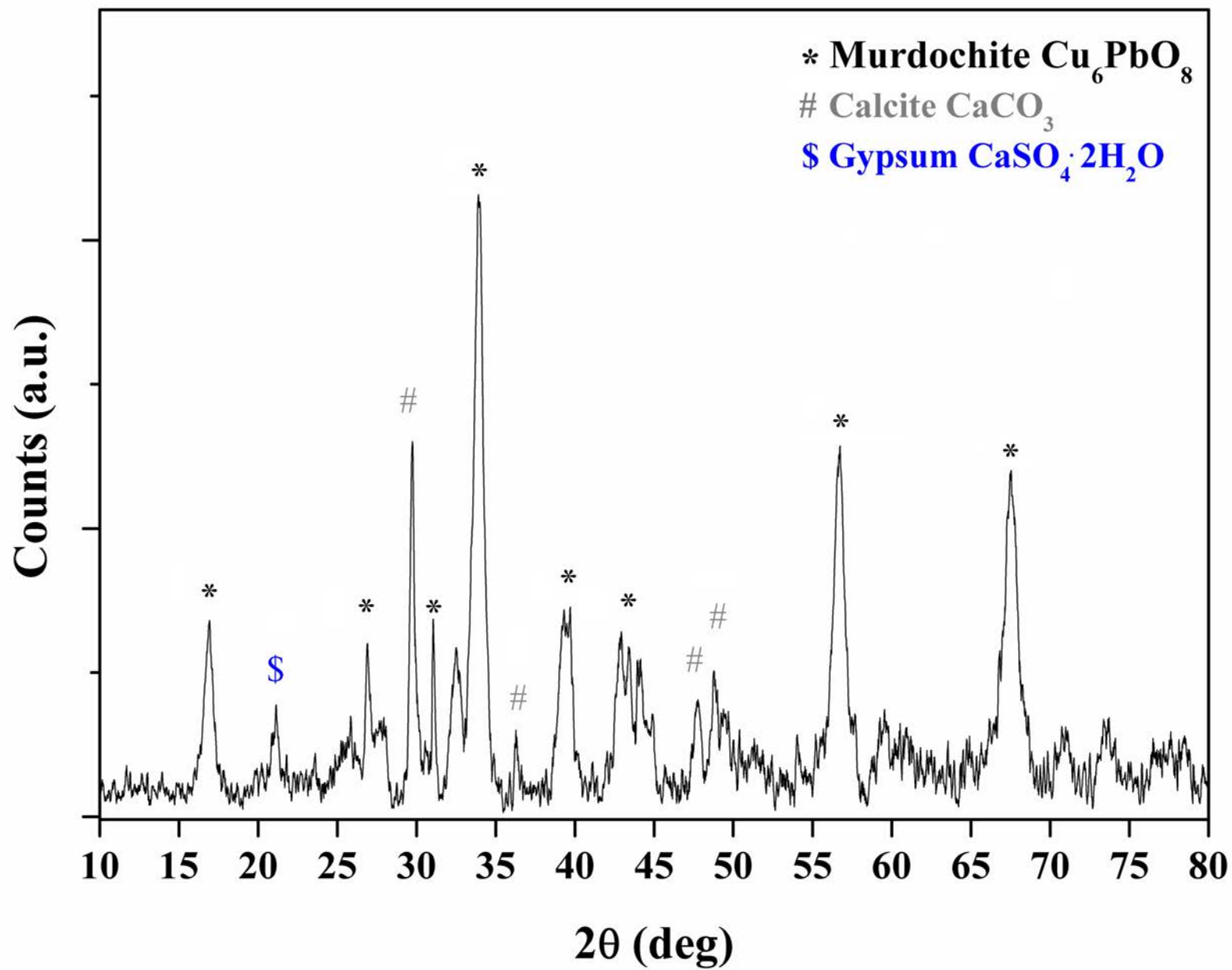












CONFLICT OF INTEREST

Manuscript title: **Archaeometric analysis of *patinas* of the outdoor copper statue *Sant'Oronzo* (Lecce, Italy) preparatory to the restoration**

Corresponding author's full name:	Alessandro Buccolieri
-----------------------------------	------------------------------

List of the authors:

N.	Author's full name
1.	Giovanni Buccolieri
2.	Alfredo Castellano
3.	Antonio Serra
4.	Giorgio Zavarise
5.	Elisabetta Palmiero
6.	Alessandro Buccolieri

All authors declare that they have no conflict of interest for the publication of the manuscript.

Lecce, 14th November 2019

Corresponding author's signature
(Alessandro Buccolieri)



AUTHORS STATEMENT FOR PUBLICATION

Manuscript title: **Archaeometric analysis of *patinas* of the outdoor copper statue *Sant'Oronzo* (Lecce, Italy) preparatory to the restoration**

Corresponding author's full name:	Alessandro Buccolieri
-----------------------------------	------------------------------

List of the authors:

No.	Author's full name
1.	Giovanni Buccolieri
2.	Alfredo Castellano
3.	Antonio Serra
4.	Giorgio Zavarise
5.	Elisabetta Palmiero
6.	Alessandro Buccolieri

Component of the research	Author's number
substantial contribution to conception and design	1 2 3 4 5 6
substantial contribution to acquisition of data	1 2 3 4 5 6
substantial contribution to analysis and interpretation of data	1 2 3 4 5 6
drafting the article	1 2 3 4 5 6
critically revising the article for important intellectual content	1 2 3 4 5 6
final approval of the version to be published	1 2 3 4 5 6

Please tick the box if the statement applies:

- to the best of your knowledge everybody who participated substantially in the study is not omitted from the article
- to the best of your knowledge, all persons listed as authors qualify for authorship

All persons who have made substantial contributions to the work but do not meet the criteria for authorship are listed in Acknowledgments section (technical help, writing assistance, general support, financial and material support)

Yes No

All persons named in the Acknowledgment section of the manuscript have given their permission to be named

Yes No

ORIGINALITY OF THE WORK STATEMENT:

- the manuscript is not previously published in the same or very similar form in other journal (previous publishing does not apply to abstract or poster presentations at a professional meeting)
- the manuscript is not currently under consideration in other journals (that does not apply for manuscripts that have been rejected by other journals)

Therefore, the manuscript has not been published previously, it is not under consideration for publication elsewhere, its publication is approved by all Authors and tacitly or explicitly by the responsible authorities where the work was carried out and, if accepted, it will not be published elsewhere in the same form in English or in any other language without the written consent of the Publisher.

Lecce, 14th November 2019

Corresponding author's signature
(Alessandro Buccolieri)



Supplementary material

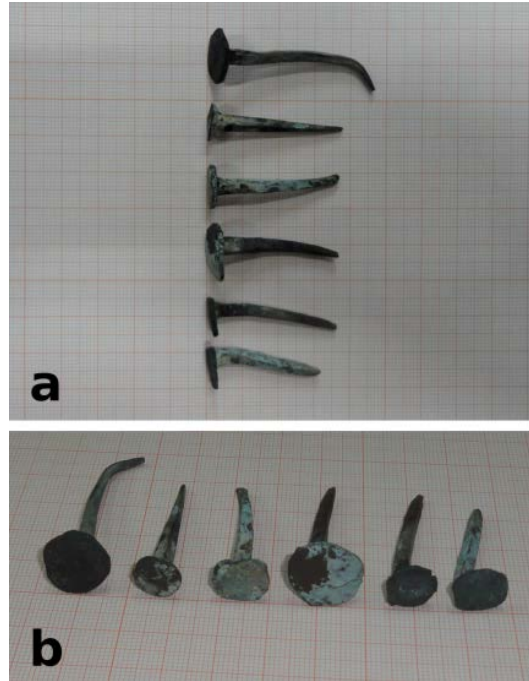


Fig. S1

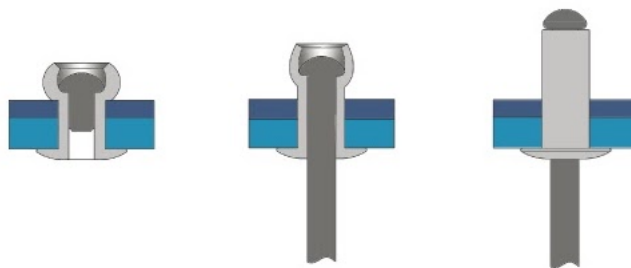


Fig. S2



Fig. S3



Fig. S4

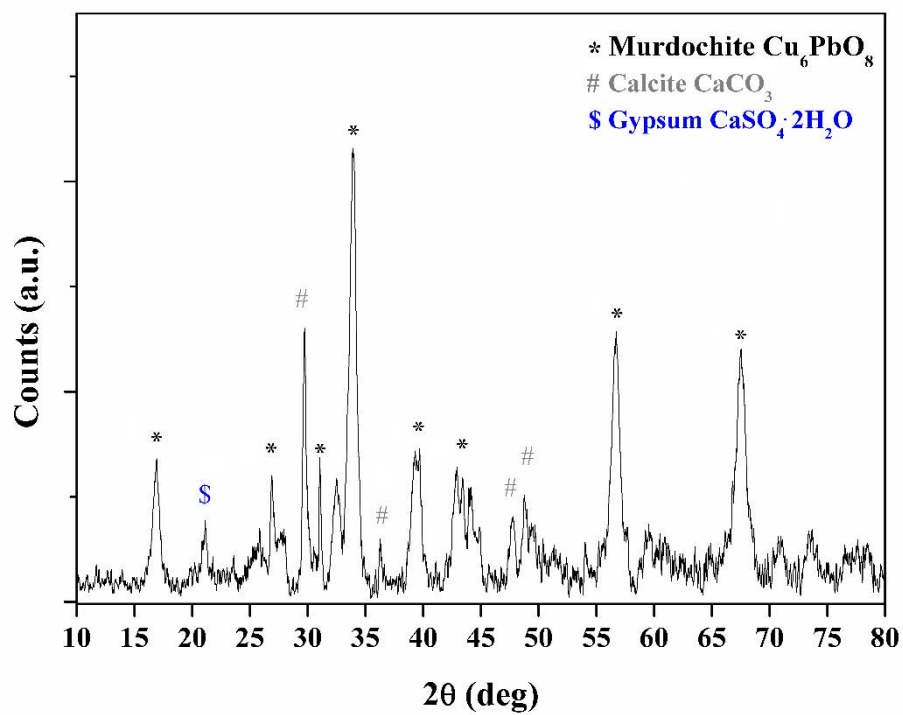


Fig. S5